Development and characterization of optimized sustained release voriconazole-loaded chitosan nanoparticles for ocular delivery

Sahar Mohammadzadeh[1], Shadab Shahsavari[2,*], Farid Karimian[3], Seyed Jamal Hashemi[3], Hamid Akbari Javar[4], Hoda Mollabagher[5]

[1] Tehran University of Medical Sciences, International Campus, Tehran, Iran

[2] Chemical Engineering Department, Varamin-Pishva Branch, Islamic Azad University, Varamin, Iran

[3] School of Public Health, Tehran University of Medical Sciences, Tehran, Iran

[4] Department of Pharmaceutics, Faculty of Pharmacy, Tehran University of Medical Sciences, Tehran, Iran

[5] Chemistry and Chemical Engineering Research Center of Iran, Tehran, Iran

HIGHLIGHTS

• Particle size of nanoparticles were reduced by decreasing concentration of chitosan at constant pH.

• At constant pH, by increasing the percentage of TPP from 5 to 20%, the EE% was raised dramatically.

• The nanoparticles had a high thermal stability that indicated well-establishment of structure.

• The release pattern indicated a very slow release of drug at each point of time from the nanoparticles.

GRAPHICAL ABSTRACT
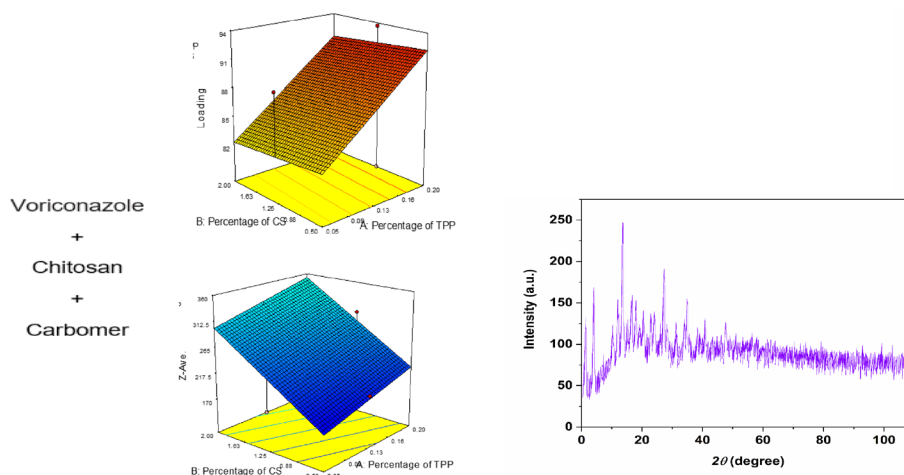
ARTICLE INFO

ABSTRACT

Voriconazole is an approved antifungal agent belonging to the triazole family. It is generally used for treating aggressive fungal infections such as invasive candidiasis or aspergillosis, as well as certain fungal infections, in immunocompromised patients. Voriconazole has an oral bioavailability of 96%, and patients can receive the medication either by oral or parenteral routes. To fabricate a topical ocular voriconazole delivery system, we prepared voriconazole-loaded chitosan nanoparticles by ionic gelation of chitosan with the addition of sodium tripolyphosphate (TPP). Three chitosan polymers with different molecular weights were tested by varying chitosan and TPP concentrations, and the produced nanoparticles were characterized by scanning electron microscopy (SEM), Fourier transform infrared spectroscopy (FT-IR), differential scanning calorimetry (DSC), and x-ray powder diffraction (XRD). The obtained data was presented into a Box-Behnken design, which showed a set of optimum parameters that would yield an optimized formulation with the most favourable properties. Subsequently, the optimized formulation was synthesized, and the voriconazole release from this formulation was monitored over 48 hr. Results showed the drug-loaded nanoparticles have high drug loading, show no burst effect, and sustain drug release for up to 48 hr. Therefore, this formulation is a potentially efficient ocular delivery system for voriconazole.

* Corresponding author: Tel.: +98912-2775093   ;   Fax: +9821-36724767   ;   E-mail address: sh.shahsavari@srbiau.ac.ir

S. Mohammadzadeh *et al.* / Journal of Particle Science & Technology 7 (2021) 1-10

1. Introduction

Heterocyclic aromatic compounds show unique antifungal and medicinal properties due to the presence of heteroatoms in their structures [1-6]. Voriconazole with the formula of (2R,3S)-2-(2,4-difluorophenyl)-3-(5-fluoropyrimidin-4-yl)-1-(1H-1,2,4-triazol-1-yl)butan-2-ol is a heterocyclic compound from a new second-generation synthetic derivative of fluconazole [7]. In addition to their antifungal activity, these compounds also have high systemic muscle penetration [8,9]. Due to the variety of drug delivery methods and the differences in costs and efficiency of drugs in different conditions, various methods have been studied and analyzed by many chemists and biological scientists in recent years [10-15]. Oral administration of voriconazole has been common but not always successful due to side effects such as liver poisoning and visual disturbances [16]. It is also expensive for the treatment of fungal keratitis [17]. Therefore, more economical methods have been examined.

Although Voriconazole has a topical effect on the cornea of rabbits [18] and horses [19], there is no formulation of this drug for human topical ocular use on the market. Eye drops are the most convenient means of ocular drug delivery. A 1% ophthalmic solution of voriconazole has been tested in patients undergoing elective eye surgery [20]. Studies have shown that despite the effectiveness of voriconazole in treating superficial eye infections, these compounds are not effective for deep-seated infections. These observations are completely consistent with the results obtained by adding 1% voriconazole solution to the eye [21]. The authors suggested that a higher voriconazole concentration might be needed to reach adequate concentrations in the eye. Therefore, researchers have been considering trastromal [22] and intracameral [23] voriconazole injection in deep cases of fungal keratitis. As such, many research groups have proposed novel formulations to improve the permeation and ocular availability of voriconazole.

To reach an effective dose of voriconazole to treat deep cases of fungal keratitis, the researchers increased the dose and found that an efficacious dose for topical ocular use of the drug needs to maintain a balance between corneal penetration, formulation stability, and no eye irritation. Several studies have been performed to improve and optimize the properties of voriconazole eye drops by the addition of hydroxypropyl beta cyclodextrin and xanthan gum [24].

Xiang-Gen *et al.* have prepared sustained release intravitreal injectable voriconazole microspheres and tested their efficacy on experimental endophthalmitis in rabbits caused by *A. fumigatus* [25]. The microspheres were prepared from poly(lactic-co-glycolic acid) (PLGA) using an oil-in-water (o/w) emulsification/solvent evaporation method. Their results showed that the inflammation could be controlled in rabbits treated with vitrectomy and microspheres containing 1.0 or 1.5 mg voriconazole as compared to the control animals in which endophthalmitis occurred in all eyes and quickly developed into pan ophthalmitis. The authors suggested that intravitreal injection of voriconazole-loaded microspheres in addition to vitrectomy can be an effective strategy for *A. fumigatus*-induced endophthalmitis in rabbits.

Another study optimized a range of microemulsion (o/w) formulations of voriconazole for ocular delivery [26]. They constructed phase diagrams to optimize the batches based on stability studies. In that study, selected batches (composed of oleic acid and isopropyl myristate as oil components with Tween 80 and propylene glycol as surfactants) showed no significant physiochemical interactions between the drug and excipient, had an acceptable viscosity and size range, and exhibited sustained release of voriconazole (>70% in 12 hr). Furthermore, an ex vivo permeation study demonstrated the microemulsion-enhanced drug flux through the cornea, and a solid lipid nanoparticle formulation has also been suggested for the ocular delivery of voriconazole [27].

Formulation optimization can increase the antifungal activity of the drug in addition to the permeability of the drug. PLGA nanoparticles loaded with voriconazole were shown to enhance its efficacy against *C. albicans* both *in vivo* and *in vitro* [28]. The use of nanoparticles in the drug delivery system increases the release power and effectiveness of the drug [29].

In this study, the design and optimization of a voriconazole drug delivery system loaded on chitosan nanoparticles with controlled release and voriconazole stability were performed. The use of a nanoparticle system for drug delivery and controlled drug release can improve efficacy and antifungal activity and reduce its invasive effect. It should be noted that a polymer matrix was used in this research due to the

therapeutic applications of this compound in humans, the biodegradation of the materials used, and their non-toxicity [30].

Considering the dependence of drug release in nanoparticle systems on the polymer composition and molecular weight, we examined chitosan polymers with different molecular weights. Three types of polymeric chitosan with different molecular weights and various concentrations of chitosan and TPP were investigated, and the final products were characterized by scanning electron microscopy (SEM), Fourier transform infrared spectroscopy (FT-IR), differential scanning calorimetry (DSC), and X-ray powder diffraction (XRD). The obtained data were fed into a Box-Behnken design in Design-Expert 7.0.0, which showed a set of optimum parameters that would yield an optimized formulation with the most favourable properties. Subsequently, the optimized formulation was synthesized, and the voriconazole release from this formulation was monitored for 48 hr.

2. Materials and Methods

2.1. Materials

Voriconazole (VRC) was supplied by AFINE Chemicals Ltd., China. Chitosan polymers (95% deacetylation, molecular weight 70 KDa, 275 KDa, 350 KDa) were obtained from Primexehf, Iceland. The other materials were of pharmaceutical and analytical grade.

2.2. Preparation of voriconazole loaded chitosan nanoparticles

Voriconazole-loaded chitosan nanoparticles were prepared according to the procedure described by Calvo et al. based on the ionic gelation of chitosan with sodium TPP anions [31]. Three different molecular weights of chitosan were tested. Briefly, chitosan and voriconazole were dissolved in 3 ml of acetic acid in an aqueous solution under magnetic stirring for 45 min at room temperature. TPP aqueous solution was added to 5 ml of chitosan-voriconazole solution, and the mixture was sonicated for 3 min. The nanosuspensions were centrifuged at 15000 g for 25 min using a Sigma centrifuge. The supernatant liquid was analyzed by a spectrophotometer (Optizen 2120 UV Plus) at 255 nm

to indirectly calculate the percentage of drug entrapment and drug loading.

2.3. Scanning electron microscopy (SEM)

SEM was used to provide pictures of nanoparticles coated with a thin gold layer under vacuum conditions to determine the morphology and surface properties of the nanoparticles.

2.4. Fourier transform infrared spectroscopy (FT-IR)

FT-IR spectroscopy was used to analyze the structure of the nanoparticles. In this method, the samples were mixed with potassium bromide under 500 atm to produce a tablet for scanning. Subsequently, the spectrum obtained from the nanoparticles was compared with those of the polymer and the drug alone.

2.5. Differential scanning calorimetry (DSC)

In general, the physiochemical changes in all materials involve thermal phenomena. These exothermal or endothermic changes are indicative of the released enthalpy during the reaction. The DSC system measures the difference in thermal flux between the sample and reference compounds relative to the temperature or time in identical heating conditions. This difference in flux is monitored by the enthalpy of the reaction and according to the enthalpy to time/temperature diagram. In this process, the sample and reference compound (air) were placed in the device oven and heated from 0 to 600 °C with an increase rate of 10 °C.min^{-1}.

2.6. X-ray powder diffraction (XRD)

The characteristic X-ray diffraction pattern generated in a typical XRD analysis provides a unique "fingerprint" of the crystals present in the sample. When properly interpreted, by comparison with standard reference patterns and measurements, this fingerprint allows identification of the crystalline form. X-ray diffraction analysis (XRD) was performed using a Shimadzu XRD diffractometer (Shimadzu Corporation, Chiyoda-ku, Tokyo, Japan) at room temperature. In all cases, Cu K_α radiation from a Cu X-ray tube (run at 15 mA and 30 kV) was used. The samples were scanned in the Bragg angle *2θ* with a range of 10 to 80.

2.7. Experimental design

The experimental design offers the possibility to rapidly and reliably understand the interactions among the different parameters involved in a multifactorial response. The number of required experiments to optimize a specific formulation can be greatly reduced using this method [32]. Therefore, the Box-Behnken design was used to determine the relationships among variables and responses. Additionally, the optimum of each variable will be obtained by differential approximation. Hence, a Box-Behnken statistical design with 3 factors and 3 levels was selected to statistically optimize the formulation parameters and evaluate the main effects, interaction effects, and quadratic effects of the formulation ingredients on the size, zeta potential, and loading of voriconazole. The experimental design allowed for the formulation of nanoparticles with the desired particle size and high entrapment efficiency. The validation test was carried out under optimum conditions of the parameters predicted by the polynomial model, and results showed that verification experiments and predicted values from fitted correlations accord very well at a 95% confidence interval. These results confirmed the validity of the models.

2.8. In-vitro drug release profiling

To obtain a calibration curve for voriconazole, solutions with concentrations of 0.5, 1, 1.5, 2, and 2.5 mg.ml^{-1} voriconazole were injected into a K-1001High performance liquid chromatography (HPLC) system (Well Chro, Germany) equipped with C18 (Column 250/4.8 Nucleosil, Macharey-Nagel, Germany) using a water-acetonitrile mobile phase (0.50-0.50) with 1 ml.min^{-1} flow rate and 29 min retention time at a wavelength of 255 nm and room temperature. All solvents were degassed for 10 min before use. Subsequently, a calibration curve with $R^2 = 0.9994$ was obtained. Afterward, the release of voriconazole from the optimized formulation was monitored for 48 hr. Experiments were performed in triplicates under optimized conditions.

3. Results and discussion

3.1. Experimental analysis

Regression analysis was used to test the adequacy of the proposed quadratic model, and the following second-order polynomial equations were derived, as shown in Eqs. (1), (2), and (3).

$$Y_1 = 73.34 + 4.58A - 0.41B - 13.96C \qquad (1)$$

$$Y_2 = 576.59 + 25.38A + 65.63B + 255C \qquad (2)$$

$$Y_3 = 41.74 + 0.99A + 0.95B + 5.44C - 0.45AB - 1.83AC - 3.2BC \qquad (3)$$

where Y_1, Y_2, and Y_3 are the predicted responses for the loading percentage of voriconazole, size, and zeta potential. A, B, and C are the coded values for the percent of TPP, percent of chitosan, and chitosan molecular weight, respectively. The statistical significance of the model equations was evaluated by the F-test for analysis of variance (ANOVA), and the model proved to be highly significant. The three-dimensional response surface curves were plotted by a statistically significant model to get a better understanding of the interaction of the affected factors (shown in Figs. 1, 2, and 3).
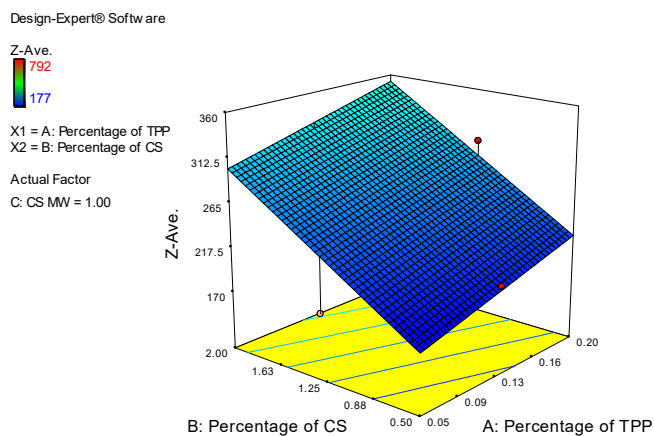
3.2. Formulation optimization

Optimization of the physical and morphological properties of the nanoparticles was done based on the data resulting from the Box Behnken response surface method. Table 1 shows the predicted optimization conditions. As shown in Table 1, the optimized condition is reached at the highest chitosan concentration level but lowest TPP concentration and chitosan molecular weight.

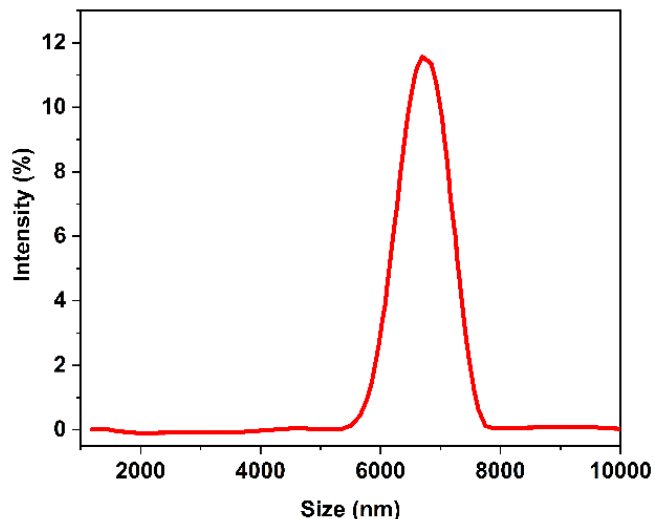Nanoparticle size distribution in the optimized
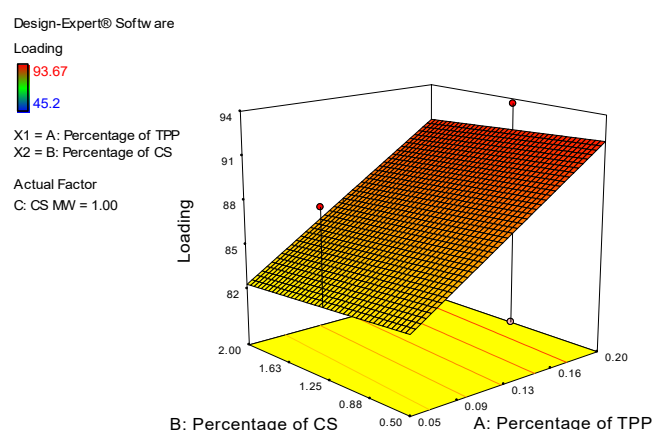
Fig. 1. Response surface plot showing the effect of factorial variables on % loading.
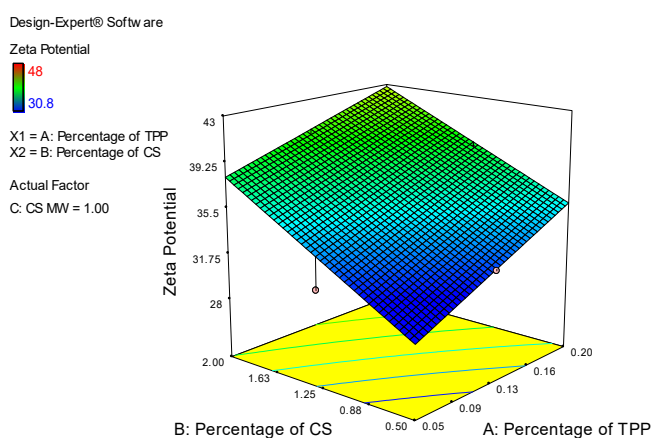
Fig. 2. Response surface plot showing the effect of factorial variables on particle size.

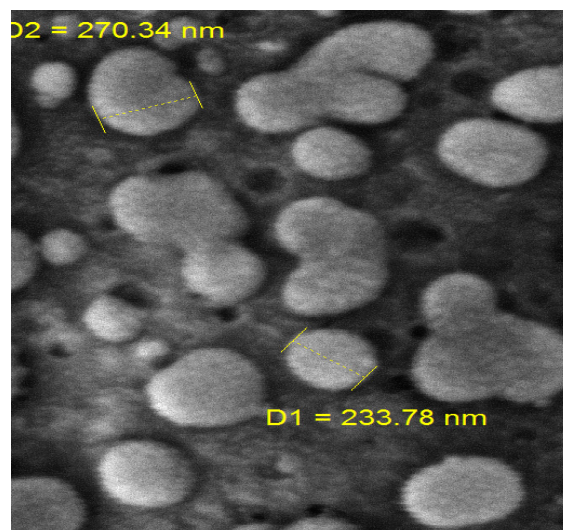**Fig. 4.** The size distribution of optimized nanoparticle formulation.

Fig. 3. Response surface plot showing the effect of factorial variables on zeta potential.

Fig. 5. The SEM image of voriconazole-loaded chitosan nanoparticles.

state (highest chitosan concentration, lowest TPP concentration, and lowest chitosan molecular weight), as measured by the dynamic light scattering (DLS) method, is displayed in Fig. 4.

3.3. Characterization of nanoparticles

3.3.1. Scanning electron microscopy (SEM)

The SEM image of the optimized nanoparticles shows that the voriconazole-loaded chitosan nanoparticles have condensed structures with a smooth spherical shape (Fig. 5).

Also as seen in Fig. 5 and Table 1, the size of the resulting particles is in the nanometer range; this shows that the chosen surfaces are suitable to examine the effect of variables of the process.

3.3.2. Fourier transform infrared spectroscopy (FT-IR)

An absorption frequency of 2987 cm^{-1} indicates the presence of the aliphatic stretch frequency of C-H.

Table 1. Optimized independent variables and the predicted responses.

Optimized independent variables			Estimated dependant variables		
TPP Concentration (A)	Chitosan Concentration (B)	Chitosan molecular weight (C)	Size (nm) (Y_1)	Zeta Potential (mV) (Y_2)	Encapsulation Efficiency (%) (Y_3)
0.2	2	1	352	42	91

The absorption frequency of 1131 cm^{-1} indicates the presence of the stretch frequency C-O, and the absorption frequency of 1277 cm^{-1} shows the aromatic stretch frequency C-N.

In the chitosan infrared spectrum (Fig. 6(a)), the absorption frequency of 1602 cm^{-1} is an indicator of the existence of the amine stretch frequency N-H, and an absorption frequency of 1327 cm^{-1} refers to the existence of the C-H frequency group. The absorption frequency of 3435 cm^{-1} indicates the presence of the stretch frequency of the amine symmetrical N-H group, and the absorption frequency of 2919 cm^{-1} shows the existence of the aliphatic C-H stretch frequency in chitosan. Absorption peaks in the range of 907 and 1150 cm^{-1} demonstrate the saccharide structure of chitosan, and the C-O stretch frequency of the chitosan structure displays strong absorption in the range of 1080 cm^{-1}.

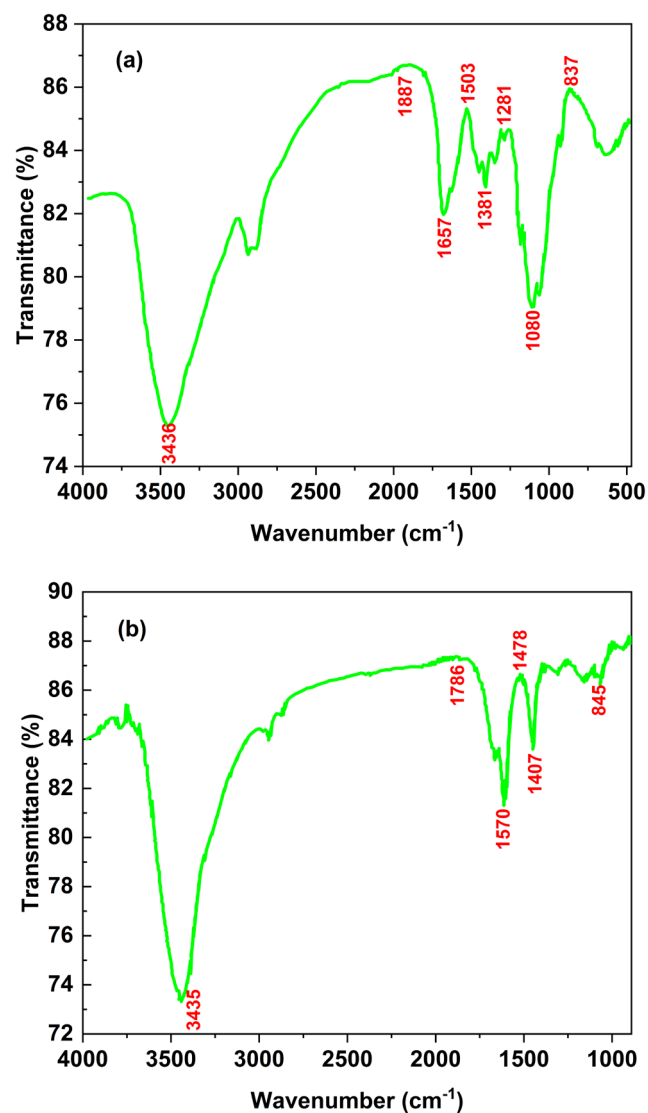The FT-IR spectrum of voriconazole-loaded chitosan nanoparticles is displayed in Fig. 6(b). Regarding the chitosan nanoparticle spectrum, the absorption frequency of 3435 cm^{-1} is evidence of the presence of the amine N-H stretch frequency, and the absorption frequency of 2920 cm^{-1} shows the existence of aliphatic C-H stretch frequency in chitosan. The absorption frequency of 1570 cm^{-1} is related to the aromatic ring C=C stretch frequency of voriconazole in the structure.

3.3.3. Differential scanning calorimetry (DSC)

DSC profile graphs corresponding to chitosan, pure voriconazole, and voriconazole-loaded chitosan nanoparticles (Fig. 7) show that in the chitosan blank spectrum, a wide exothermic peak at 117 °C and an endothermic peak at ~310 °C, which agrees with the observations in reference databases. Sharp exothermic at the 137 °C peak refers to voriconazole in Fig. 7(b). In Fig. 7(c), the two exothermic and endothermic peaks at 117 and 310 °C indicate the existence of chitosan, and the exothermic peak transfer from 120 to 160 °C signifies the loading of the voriconazole drug in chitosan nanoparticles.

3.3.4. X-ray powder diffraction (XRD)

The X-ray powder diffractogram (XRD) technique demonstrates and confirms the loading of the drug on nanoparticles.

As it was clear in Fig. 8(c), the chitosan indicator peaks overlap with the drug indicator peak, chitosan peak widening at $2\theta = 22$ is obvious, and the drug peak intensities are high, indicating the existence of high levels of the drug in the structure of the nanoparticles.

3.4. In-vitro drug release profiling

3.4.1. In-vitro release study of voriconazole from optimized nanoparticles

The voriconazole release plot of the optimized nanoparticle formulation has been shown based on the percentage of the drug released in time, in phosphate buffer media (pH=6.8), and with and without a carbomer matrix (Fig. 9). As shown in Fig. 9(a), during the first 30 min of release, no burst release from nanoparticles is observed, which indicates suitable friction between
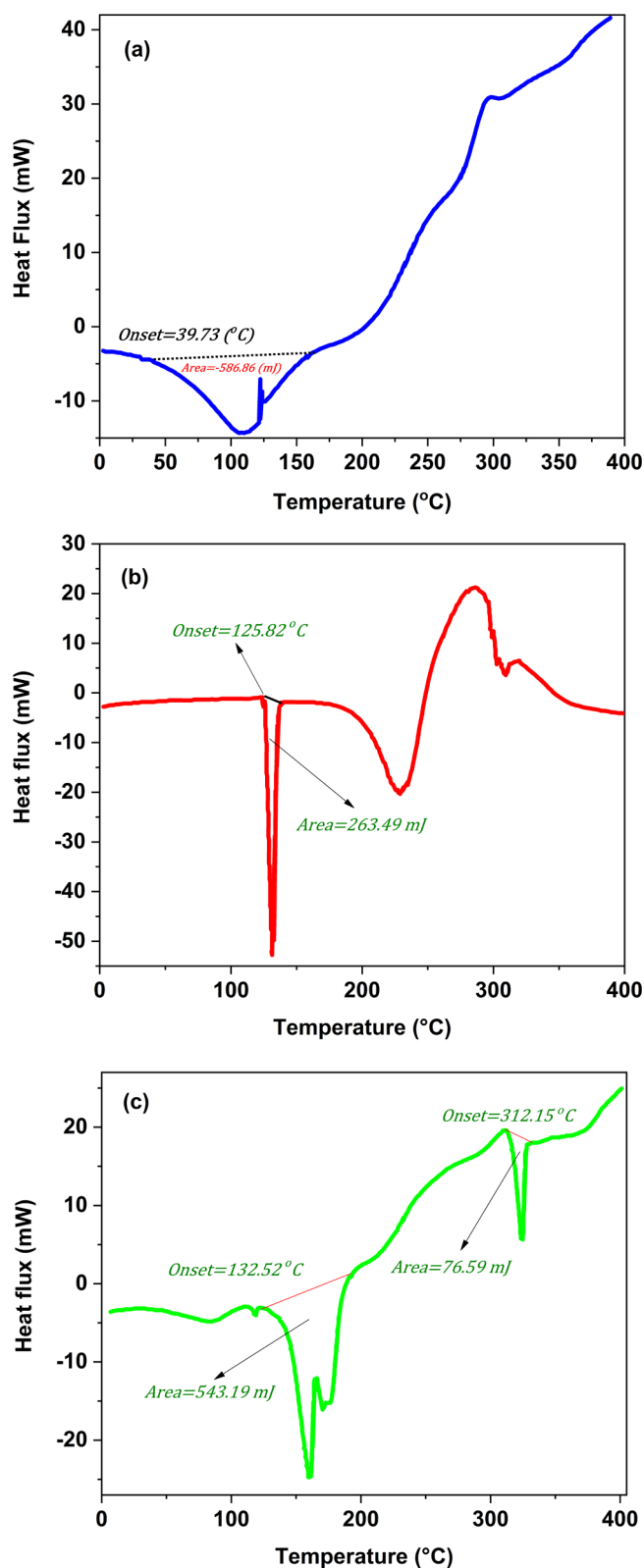

Fig. 6. FT-IR spectrum of (a) chitosan and (b) voriconazole-loaded chitosan nanoparticles.

Fig. 7. DSC profile of (a) chitosan, (b) Pure voriconazole, and (c) voriconazole-loaded chitosan nanoparticles.
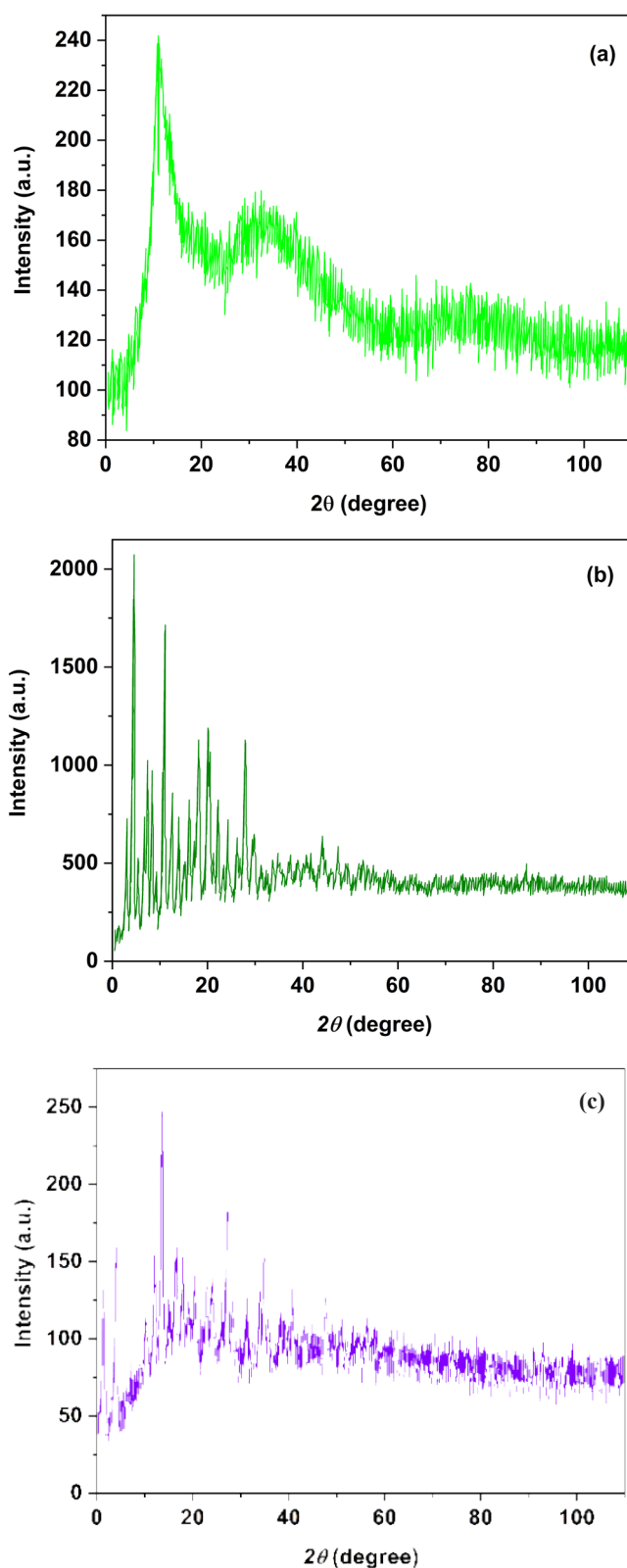

Fig. 8. XRD graph of (a) chitosan, (b) voriconazole, and (c) chitosan-voriconazole nanoparticles.

the voriconazole and chitosan particles. Almost 26.27% of the drug is released during the first hour of release, and then the drug release from nanoparticles gradually increases. As shown in Fig. 9(a), the highest voriconazole release level in the media was 71.52% in 48 hours, and

the release model shows a very slow release from the nanoparticles at any given time. Finally, after 48 hr, a strong polymer network forms due to the hypothetical friction between the chitosan and TPP nanoparticles, and voriconazole molecules are captured in this matrix,
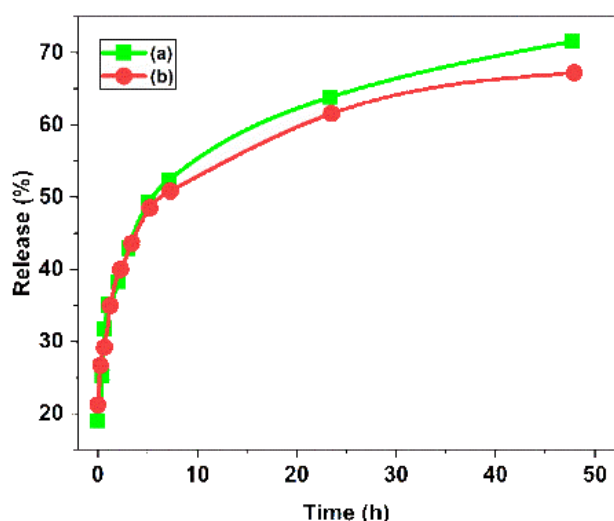
Fig. 9. (a) Drug release from voriconazole-loaded chitosan nanoparticles and (b) Voriconazole release from nanoparticles with 1% carbomer matrix.

which decreases the speed of voriconazole release. Since one of the objectives of using nanoparticles in pharmaceutical applications is to sustain drug release over time, the nanoparticles fabricated in this study can be potentially used as efficient ocular drug delivery systems for voriconazole.

Furthermore, we examined the *in vitro* release profile of voriconazole from optimized nanoparticles in a 1% concentration of carbomer matrices in a phosphate buffer solution (Fig. 9(b)). The release pattern indicates the sustained and controlled release of voriconazole from nanoparticles at any given time, and no burst release from the nanoparticles exists. This release pattern may refer to the formation of a strong polymer network in which drug release happens in a controlled and stable manner.

3.4.2. Drug release modelling characterization

To estimate the value of n and determine a mathematical model defining voriconazole release from nanoparticles, the Peppas equation graph *log* (M_t/M_∞) was drawn against *log t*, and the slope (n) was calculated. Since the calculated n value (0.21) is smaller than 0.43, the drug release from nanoparticles follows the Fickian law.

4. Conclusion

The present study demonstrated that the molecular weight of chitosan, as well as chitosan content and TPP content, can influence the particle size, drug entrapment efficiency, and loading capacity of voriconazole-loaded chitosan nanoparticles. The size of the prepared nanoparticles ranged from 177 to 792 nm, with PDIs lower than 0.3. Moreover, nanoparticles exhibited a high positive zeta potential.

According to numerical optimization, the maximum predicted amount of loading, minimum predicted size, and zeta potential are 91.46, 352.58, and 42.81, respectively. The morphological study of the nanoparticles indicates the formation of spherical nanoparticles with smooth surfaces. Thermal analysis shows nanoparticle stability at temperatures higher than 200 °C.

The *in vitro* release study with optimized nanoparticle formulation showed the absence of burst release and the presence of suitable friction between chitosan and voriconazole polymers, which contributes to a sustained drug release. According to modelling studies, drug release from the nanoparticles followed a first-order kinetic model with a Fickian mechanism. Based on the favorable properties of the fabricated nanoparticles, this optimized formulation could be a potentially efficient ocular voriconazole delivery system for the treatment of fungal keratitis. In future studies, we aim to investigate the penetration and efficacy of voriconazole-loaded chitosan nanoparticles.

Conflict of interest

The authors declare that they have no conflict of interest.

References

[1] H. Mollabagher, S. Taheri, M. Majid Mojtahedi, S. Seyedmousavi, Cu-metal organic frameworks (Cu-MOF) as an environment-friendly and economical catalyst for one pot synthesis of tacrine derivatives, RSC Adv. 10 (2020) 1995-2003.

[2] H. Mollabagher, S. Taheri, An efficient method for the synthesis of neuroprotective drug riluzole, 20th Iranian chemical congress, Iran, 2018.

[3] G. Mohammadi Ziarani, H. Mollabagher, N. Lashgari, A. Badiei, One-pot solvent-free synthesis of pyranonaphthoquinone-fused spirooxindoles catalyzed by SBA-IL, Sci. Iran. 25 (2018) 3295-304.

[4] G. Mohammadi Ziarani, H. Mollabagher, P. Gholamzadeh, A. Badiei, F. Yazdian, Synthesis of

the biologically active henna based benzochromene derivatives using ionic liquid functionalized SBA-15 as a nanoreactor, Iranian J. Catal. 8 (2018) 59-67.

[5] S.Y. Afsar, G.M. Ziarani, H. Mollabagher, P. Gholamzadeh, A. Badiei, A.A. Soorki, Application of SBA-Pr-SO$_3$H in the synthesis of 2, 3-dihydroquinazoline-4 (1*H*)-ones: Characterization, UV–Vis investigations and DFT studies, J. Iranian Chem. Soc. 14 (2017) 577-583.

[6] T. Ahmadi, G.M. Ziarani, P. Gholamzadeh, H. Mollabagher, Recent advances in asymmetric multicomponent reactions (AMCRs), Tetrahedron-Asymmetry, 28 (2017) 708-724.

[7] D. Al-Badriyeh, C.F. Neoh, K. Stewart, D.C. Kong, Clinical utility of voriconazole eye drops in ophthalmic fungal keratitis, Clinical Ophthalmology (Auckland, NZ) 4 (2010) 391-405.

[8] S. Hariprasad, W. Mieler,T. Lin, W. Sponsel, J. Graybill, Voriconazole in the treatment of fungal eye infections: a review of current literature, Brit. J. Ophthalmol. 92 (2008) 871-878.

[9] U.V. Jurkunas, D.P. Langston, K. Colby, Use of voriconazole in the treatment of fungal keratitis, Int. Ophthalmol. Clin. 47 (2007) 47-59.

[10] K. Khoshnevisan, H. Maleki, H. Samadian, S. Shahsavari, M.H. Sarrafzadeh, B. Larijani, *et al.*, Cellulose acetate electrospun nanofibers for drug delivery systems: Applications and recent advances, Carbohyd. Polym. 198 (2018) 131-141.

[11] S. Shahsavari, L.R. Shirmard, M. Amini, F.A. Dokoosh, Application of artificial neural networks in the design and optimization of a nanoparticulate fingolimod delivery system based on biodegradable Poly (3-Hydroxybutyrate-Co-3-Hydroxyvalerate), J. Pharm. Sci. 106 (2017) 176-182.

[12] S. Seifirad, H. Karami, S. Shahsavari, F. Mirabasi, F. Dorkoosh, Design and characterization of mesalamine loaded nanoparticles for controlled delivery system, Nanomed. Res. J. 1 (2016) 97-106.

[13] S. Shahsavari, E. Vasheghani-Farahani, M. Ardjmand, F. Abedin Dorkoosh, Modeling of drug released from acyclovir nanoparticles based on artificial neural networks, Lett. Drug Des. Discov. 11 (2014) 174-183.

[14] S. Shahsavari, E. Vasheghani-Farahani, M. Ardjmand, F. Abedin Dorkoosh, Design and characterization of acyclovir loaded nanoparticles for controlled delivery system, Curr. Nanosci. 10

(2014) 521-531.

[15] S. Shahsavari, G. Bagheri, R. Mahjub, R. Bagheri, M. Radmehr, M. Rafiee-Tehrani, *et al.*, Application of artificial neural networks for optimization of preparation of insulin nanoparticles composed of quaternized aromatic derivatives of chitosan, Drug Res. 64 (2014) 151-158.

[16] A.J. Ullmann, Review of the safety, tolerability, and drug interactions of the new antifungal agents caspofungin and voriconazole, Curr. Med. Res. Opin. 19 (2003) 263-271.

[17] A. Stewart, R. Powles, M. Hewetson, J. Antrum, C. Richardson, J. Mehta, Costs of antifungal prophylaxis after bone marrow transplantation, Pharmacoeconomics, 8 (1995) 350-361.

[18] W. Sponsel, N. Chen, D. Dang, G. Paris, J. Graybill, L.K. Najvar, *et al.*, Topical voriconazole as a novel treatment for fungal keratitis, Antimicrob. Agents Ch. 50 (2006) 262-268.

[19] A.B. Clode, J.L. Davis, J. Salmon, T.M. Michau, B.C. Gilger, Evaluation of concentration of voriconazole in aqueous humor after topical and oral administration in horses, Am. J. Vet. Res. 67 (2006) 296-301.

[20] D. Lau, M. Fedinands, L. Leung, R. Fullinfaw, D. Kong, G. Davies, *et al.*, Penetration of voriconazole, 1%, eyedrops into human aqueous humor: a prospective open-label study, Arch. Ophthalmol.-Chic 126 (2008) 343-346.

[21] G.A. Vemulakonda, S.M. Hariprasad, W.F. Mieler, R.A. Prince, G.K. Shah, R.N. Van Gelder, Aqueous and vitreous concentrations following topical administration of 1% voriconazole in humans, Arch. Ophthalmol.-Chic 126 (2008) 18-22.

[22] N. Sharma, P. Agarwal, R. Sinha, J.S. Titiyal, T. Velpandian, R.B. Vajpayee, Evaluation of intrastromal voriconazole injection in recalcitrant deep fungal keratitis: case series, Brit. J. Ophthalmol. 95 (2011) 1735-1737.

[23] K.H. Kim, M.J. Kim, H. Tchah, Management of fungal ocular infection with topical and intracameral voriconazole, J. Korean Ophthalmol. Soc. 49 (2008) 1054-1060.

[24] S. Malhotra, A. Khare, K. Grover, I. Singh, P. Pawar, Design and evaluation of voriconazole eye drops for the treatment of fungal keratitis, J. Pharm. (Cairo) 2014 (2014) 490595.

[25] W. Xiang-Gen, Y. Li-Na, X. Meng, J. Hao-Ran,

Anti-infectious activity of intravitreal injectable voriconazole microspheres on experimental rabbit fungal endophthalmitis caused by Aspergillus fumigatus, J. Pharm. Sci. 100 (2011) 1745-1759.

[26] R. Kumar, V. Sinha, Preparation and optimization of voriconazole microemulsion for ocular delivery, Colloid. Surface. B, 117 (2014) 82-88.

[27] R. Kumar, V. Sinha, Fabrication of voriconazole solid lipid nanoparticles for effective ocular delivery, Value Health, 17 (2014) A613.

[28] H. Peng, X. Liu, G. Lv, B. Sun, Q. Kong, D. Zhai, Q. Wang, W. Zhao, G. wang *et al.*, Voriconazole into PLGA nanoparticles: Improving agglomeration and antifungal efficacy, Int. J. Pharm. 352 (2008) 29-35.

[29] P. Pawar, H. Kashyap, S. Malhotra, R. Sindhu, Hp-β-CD-voriconazole *in situ* gelling system for ocular drug delivery: *in vitro*, stability, and antifungal activities assessment, Biomed. Res. Int. 2013 (2013) 341218.

[30] A.J. Wagstaff, D. Faulds, K.L.Goa, Aciclovir. A reappraisal of its antiviral activity, pharmacokinetic properties and therapeutic efficacy, Drugs, 47 (1994) 153-205.

[31] P. Calvo, C. Remuñan-López, J.L. Vila-Jato, M.J. Alonso, Chitosan and chitosan/ethylene oxide-propylene oxide block copolymer nanoparticles as novel carriers for proteins and vaccines, Pharm. Res. 14 (1997) 1431-1436.

[32] Ü. Açıkel, M. Erşan, Y.S. Açıkel, Optimization of critical medium components using response surface methodology for lipase production by Rhizopus delemar, Food Bioprod. Process. 88 (2010) 31-39.